




# A hydrogel-based phantom of the brain tissue aimed at modelling complex metabolic transport processes

Anastasia S. Vanina<sup>1,a</sup>, Alexander V. Sychev<sup>2,b</sup>, Anastasia I. Lavrova<sup>3,4,c</sup>, Pavel V. Gavrilov<sup>3,d</sup>, Polina L. Andropova<sup>5,e</sup>, Elena V. Grekhnayova<sup>1,f</sup>, Tatiana N. Kudryavtseva<sup>1,g</sup>, and Eugene B. Postnikov<sup>6,7,h</sup> 

<sup>1</sup> Laboratory of Organic Synthesis, Kursk State University, Radishcheva st. 33, Kursk 305000, Russia

<sup>2</sup> Research Center for Condensed Matter Physics, Kursk State University, Radishcheva st. 33, Kursk 305000, Russia

<sup>3</sup> Saint-Petersburg State Research Institute of Phthiopolmonology, Lygovsky av. 2-4, Saint Petersburg 191036, Russia

<sup>4</sup> Faculty of Medicine, Saint-Petersburg State University, Universitetskaya emb 7-9, Saint Petersburg 199034, Russia

<sup>5</sup> N. P. Bechtereva Institute of the Human Brain of the Russian Academy of Sciences, Akad. Pavlov st., 9, Saint Petersburg 197376, Russia

<sup>6</sup> Department of Theoretical Physics, Kursk State University, Radishcheva st., Kursk 305000, Russia

<sup>7</sup> Institute of Physics, Saratov State University, Astrakhanskaya st. 83, Saratov 410012, Russia

Received 3 October 2022 / Accepted 28 November 2022 / Published online 9 December 2022

© The Author(s), under exclusive licence to EDP Sciences, Springer-Verlag GmbH Germany, part of Springer Nature 2022

**Abstract** Amongst the modern problems of brain physiology, special attention is drawn to the transport processes in the brain's extracellular space, which are crucial for understanding metabolic exchange, waste clearance, etc. At the same time, the complexity of direct registration of such processes in vivo forms a demand for developing artificial phantoms with properties resembling the brain's parenchyma as models suited for testing different physical approaches to describing the respective spread of substances. Here we describe a novel hydrogel material with composition and structure adjusted to this goal. The phantom comprises a collagen network with the addition of lipids and catches water content close to that of the brain. The results of electron microscopy and computer tomography studies as well as exploration of peculiarities of the fluorescent marker spread argue that this compound material is prospective for its use for mimicking the brain's tissue.

## 1 Introduction

Recently, there is more and more substantiated understanding that brain's physiology cannot be considered only within the frames of a set of neuronal cell, and one should necessarily take into account processes taking place in the brain's extracellular space (ESC), which is even characterised as the “final frontier of neuroscience” [1]. These micro-environments with extremely complex structure filled by interstitial fluids surround all cells of the central nervous system and maintain their activity, assure clearance of the waste metabolites, etc. but is still not comprehensively explored [2].

In particular, one of the most disputable modern questions is the type of solute transport though the parenchyma respectively to existence either of directed flows (so-called “glymphatic hypothesis” first proposed in the work [3]) or purely diffusive transport (which, however, may have non-conventional features not described by a single Gaussian distribution due to complexity of the ESC, see e.g. [4, 5]). The overview of the recent state-of-the-art on this controversial topic can be found, e.g. in the reviews [6–9].

Note that the direct experimental characterisation of the brain's extracellular space (ECS), which is the main route for metabolic transport in the brains, as well as quantification the diffusion process in vivo is a complicated task [10]. Moreover, the ECS may be affected by a variety of cellular metabolic processes, physiological conditions and neuronal activity [11, 12]. Therefore, physical modelling of transport (primary, diffusional) processes in such a tissue requires the development of simplified phantoms resembling the composition and complex structure of the brain's parenchyma but simultaneously able to be controlled by an observer [13].

<sup>a</sup> e-mail: [vanina.nast.05@gmail.com](mailto:vanina.nast.05@gmail.com)

<sup>b</sup> e-mail: [sychev1113@gmail.com](mailto:sychev1113@gmail.com)

<sup>c</sup> e-mail: [aurebours@googlemail.com](mailto:aurebours@googlemail.com)

<sup>d</sup> e-mail: [spbniifrentgen@mail.ru](mailto:spbniifrentgen@mail.ru)

<sup>e</sup> e-mail: [polin.and@icloud.com](mailto:polin.and@icloud.com)

<sup>f</sup> e-mail: [grekhnayovaev@yandex.ru](mailto:grekhnayovaev@yandex.ru)

<sup>g</sup> e-mail: [kudr15@yandex.ru](mailto:kudr15@yandex.ru)

<sup>h</sup> e-mail: [postnikov@kursksu.ru](mailto:postnikov@kursksu.ru) (corresponding author)

The conventional reference material used for studies of the diffusion processes in the brain is the agarose gel [14–16]. It has typical diffusion coefficients close by value to the brain's one easily controlled by the simple change of agarose's concentration, allows easy registering the diffusion process using fluorescent markers, has microscopic poroelasticity at high concentrations, etc. At the same time, this medium has certain drawbacks as high meso- and macro-scopic uniformity, too fluid consistency (i.e. mechanical mismatch to the brain), impossibility to create pathways imitating, e.g. wider peri-vascular space.

For this reason, there is a recent demand for more realistic brain-tissue-like biomaterials [17]. Amongst them, hydrogels, which are three-dimensional cross-linked insoluble hydrophilic polymer meshes able to absorb large amounts of water or biological fluid in interconnected microscopic pores looks as promising media [13, 18–20]. Due to the possibility to control polymers linking provides an opportunity to resemble the extracellular matrix (ECM) and simultaneously reproduces mechanical viscoelasticity of the soft tissue, i.e. to combine both micro- and macro-scopic properties of the brain. Due to relative transparency, it is possible to carry out noninvasive optical measurements within the samples and, therefore, to test different models of the diffusion process as influenced of the heterogeneity of hydrogels at different scales, which can be controlled during their fabrication.

Thus, the principal goal of the present work is in the development of a variant of the novel material, which should resemble complex structural properties of the brain's parenchyma and studying its structural and transport-supporting properties in comparison with realistic biological data. Such a material should combine gel-like elastic consistency, bind a significant amount of water (thus, to be a hydrogel) and have a complex network-like structure of its matrix for reproducing peculiarities of the tissue most valuable for studying transport properties related to the metabolic spread in the brain's parenchyma.

## 2 Hydrogel material

### 2.1 Premises

It is known [21] that the brain's chemical content consists of approximately (in per cents of the tissue mass) 84/70% of water in the grey/white matter and, in the rest dry compounds 8/8% of proteins, 5/17% of lipids, and 1/2% mineral substances. Thus, the model brain's phantom should contain a network-like structure mimicking the matrix of the tissue, water-soluble and -insoluble proteins and a lipid component. An addition, the formed gel-like substance should bind a sufficient amount of water. The collagen-based hydrogel is a promising candidate for this goal. Moreover, collagen extracted from fish skin is more suitable for brain models than, for example, collagen from bovine shin splits

because of the unique fibrillar structure of the fish's skin matrix. The latter includes the shorter length of the protein fibrils and lower molecular weight, as well as the unique amino acid composition.

### 2.2 Fabrication

As a source for producing collagen-based matrix, the skin of scaleless fish, North African sharp-toothed catfish *Clarias gariepinus*. The absence of scales in this species allows a considerable simplification of the preliminary preparation of raw materials, which was factually reduced to mechanical cleaning of the skin with a suspension of sodium bicarbonate. Pre-washed and degreased raw material was ground manually or with a laboratory knife mill SM-3 and then subjected to bleaching with an alkaline solution of hydrogen peroxide.

The pre-treated peroxide-shell skin mainly contains collagen with a small admixture of hyaluronic acid. To loosen the collagen fibrils, the discoloured collagen-containing material was treated with citric acid. The resulting mass was treated with 27 kHz ultrasound for 5 min and then cooled. This treatment was repeated several times and the mass was homogenised. After this process, the macromolecules of the polymers were partially degraded that resulted in a presence of a certain amount of water-soluble proteins.

To simulate lipids included into the content of the neuroglial layers of myelin covering the neuronal network, lecithin with high phosphatidylcholine content was added to the working solution slowly with intensive stirring.

A composition with a mass concentration of collagen of 2% was used as a working gel. To stabilise it, the standard material for cross-linking collagen structures, a concentrated glutaraldehyde solution, was added in an amount of 10% of the collagen mass.

As a result, the gel contains collagen imitating a structurally supporting, water-insoluble component, water-soluble proteins formed as a result of ultrasonic destruction of collagen, as well as phospholipids and traces of carbohydrates, which, in general, corresponds to the approximate chemical composition of the brain.

## 3 Structural properties

### 3.1 Scanning electron microscopy (dry sample)

As the first step for characterising the structure of the synthesised hydrogel, we carried out an analysis of its collagen matrix with the scanning electron microscope Quanta FEG 650. Figure 1 illustrates the obtained images of the dried hydrogel's surface, which allows exploration of the collagen network morphology. One can see that it demonstrates a multiscale porosity varying from tenth  $\mu\text{m}$  to tenth nm. This feature already resembles the range of spatial scales of the brain's ESC

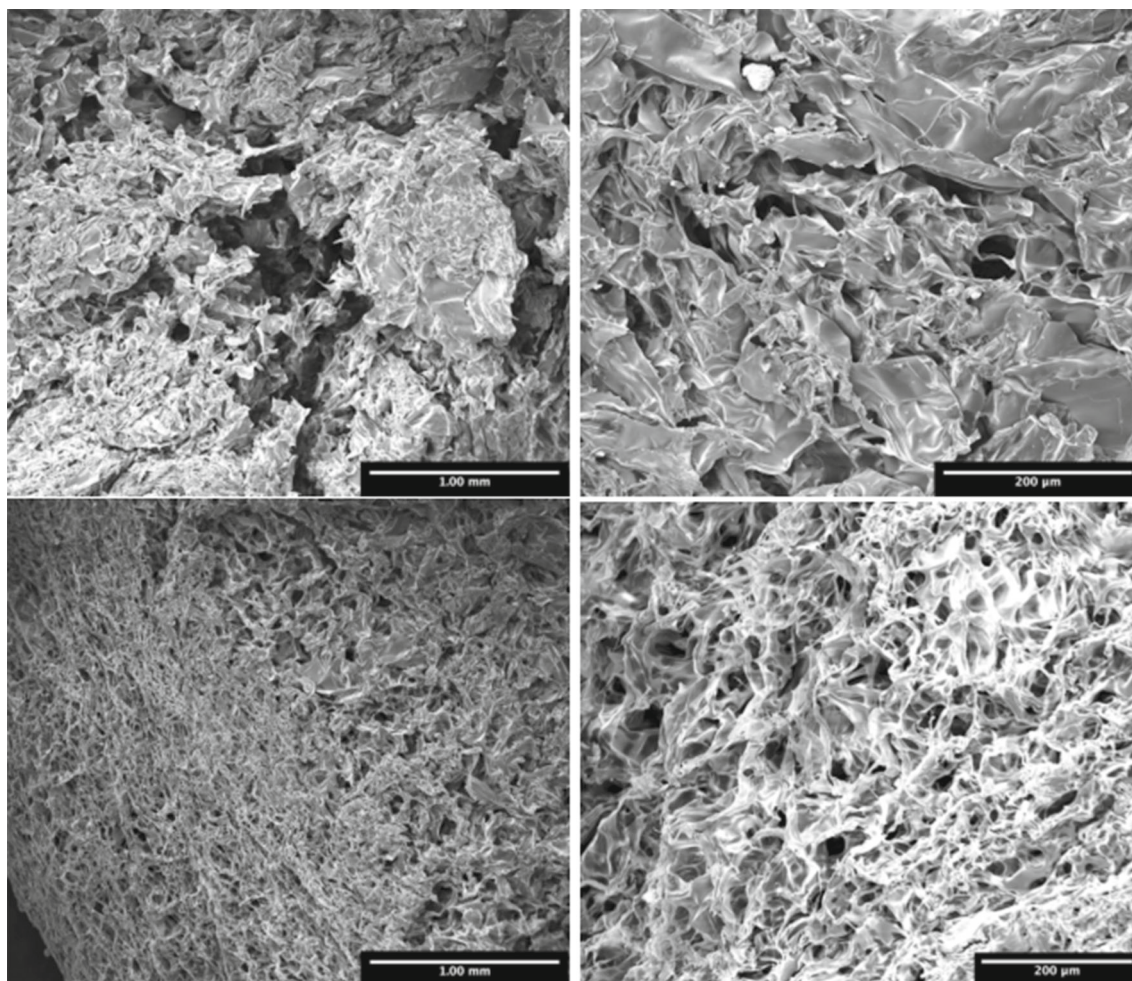


**Fig. 1** The structure of the collagen matrix in the dried obtained with SEM at different levels of resolution

[2], and, therefore, when these pores will be filled with water or physiological solution-like fluid, one can expect the the transport of molecular markers or nanoparticles will follow the same pattern of diffusion in inhomogeneous medium with traps and barriers [22].

It worth noting also similarities between the dried phantom shown in Fig. 1 and native pig brain tissue and the matrigel formed after decellularisation both consisting of a network of fibres forming the qualitatively similar image as can be found in the work [23].

### 3.2 Computed tomography (wet sample)

The water-contained sample of the hydrogel was examined using a Canon AQUILION ONE 320 CT scanner. Due to the non-standard nature of the object, the optimum scanning settings were selected in the manual mode. The best visualisation of the object was obtained with the following parameters: the tube peak voltage (KVP: kilovolt in peak) 135 kVp, X-Ray Tube Current 20 mA, and Exposure 7 mAs. Also taking into account that the minimum detector size is 0.5 mm, we used a

dimensionless Spiral Pitch Factor of 0.638 and reconstructed slices with a thickness of 0.25 mm. The convolution Kernel FC49 was used for the image processing. This kernel was selected from those available in the base of Canon AQUILION ONE 320. For optimal viewing, the window with the parameters of window level (WL) and window width (WW) WL = 128, WW = 256 (both in Hounsfield units) was selected.

Figure 2 illustrates the 3D structural features revealed via the postprocessing of the obtained images in the “Brain” mode (Fig. 2A–D) and in the “Heart” mode (Fig. 2E–H) from the base of Canon AQUILION ONE 320 predefined settings. The first set of images highlights the collagen contents as brighter regions on the dark background of the water content. One can clearly see the network-like structure almost uniformly spread over the whole sample, which looks similar to a granular picture seen in CT images of the real brain [24, 25]. Thus, the images, which we obtained for the synthesised hydrogel argued in favour of its structure, which comprises the collagen barriers (and traps, when collagen surrounds the water drop) between water routes, where the diffusion of substances can easily occur. In other word, it is a clear example of a phantom for

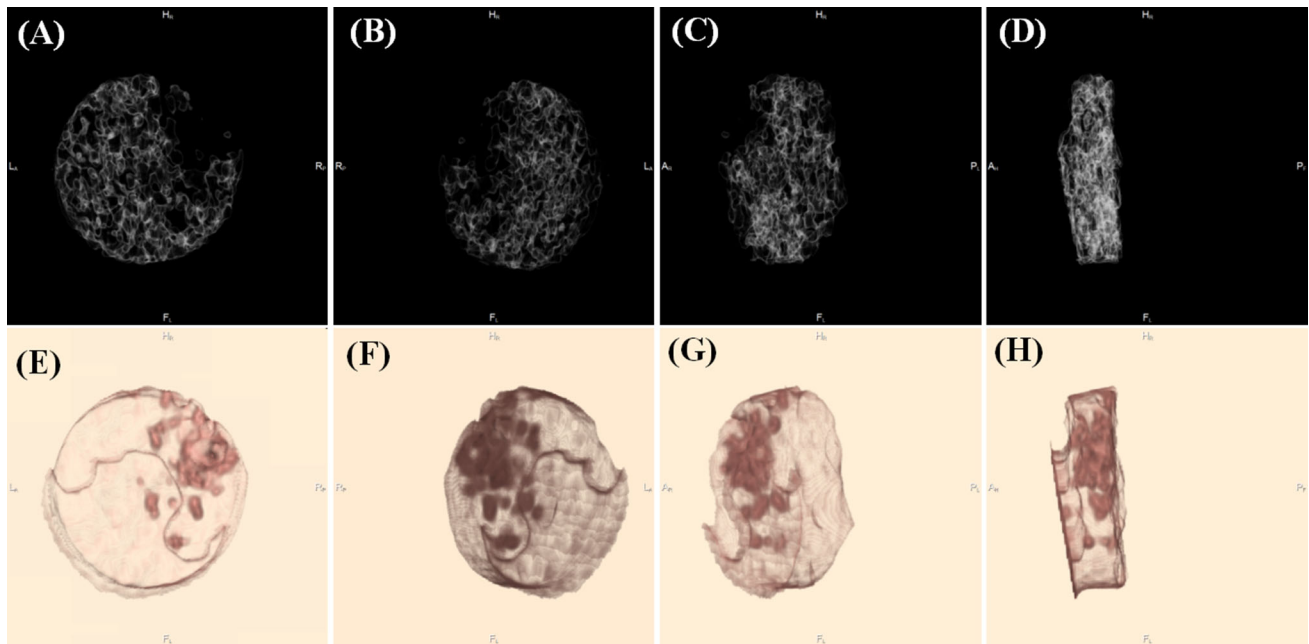


**Fig. 2** The processed computed tomography images of the hydrogel turned at different angles: **A–D** in the mode highlighting the collagen matrix; **E–H** in the mode highlighting the lipid content

the biomimetic compartmentalised medium [26], which attracts an active attention in the modern theory of complex diffusion processes.

The second set of images (Fig. 2E–H) highlights the distribution of lipids in the bulk of the hydrogel. In addition to fine-dispersed fraction on the surface of the collagen cells, one can see also the presence of localised larger lipid drops, which are distributed anisotropically. One will see in the next section devoted to the analysis of the fluorescent marker spread some peculiarities, which can be associated with this distribution.

#### 4 Transport properties: recordings and analysis

The records of the marker's spread in the hydrogel were carried out as follows: the solution contained fluorescence marker was injected into the gels' bulk by the vertically inserted needle, which was extracted after. Thus, a thin vertical channel filled by the fluorescent solution was formed, and the further process goes in radial direction from this line, i.e. it can be considered as quasi-two-dimensional one and going in a passive, i.e. diffusive, mode.

An aqueous solution of 9-Oxo-9,10-dihydroacridine-2-sulfonic acid was used as a fluorescent marker excited by the uniform ultraviolet illumination at the line  $\lambda = 366$  nm. Figure 3 demonstrates the reflective blue glow of the spread marker. These sets of photos explore the gel's cross sections made after study of the transport,

and one can see that it is already possible to the processes of vertical redistribution and considered an effective 2D picture from above.

Video recordings were by the camera of iPhone 7 with an additional lens during 17 min after the needle's removal. The recorded video was split into separate frames using standard tools of MATLAB, and the blue channel intensity was extracted as corresponding to the density distribution of the fluorescent marker, see Fig. 4 exemplifying the spread for several time moments.

It should be pointed out that during the step of injection, some part of the solution was spread under the excess pressure that formed a non-point initial distribution, see e.g. the image Fig. 4A, which was taken after 1 min after the needle's extraction. Visually exploring Fig. 4, one can see that the initial spot is irregular. It has a slightly ellipsoidal shape and, additionally, there is a protuberance formed, probably, by the fast percolation through some channel in the gel structure simplified by the presence of lipid inclusions visible in Fig. 2E–H. The comparison of Figs. 2E and 4A supports this conclusion because of the protuberance directed towards the highly concentrated lipid-originated region. Note that such kind of anisotropy is already known in the brain tissue, affecting diffusion of substances in the extracellular space as detected by the photobleaching experiments with fluorescent dyes [27], Integrative optical imaging (IOI) method with fluorophore-labelled molecules [28], and by the dynamic MRI mapping of contrast agent concentrations [29].

Thus, to investigate the temporal evolution of the marker's distribution, we considered not only the full

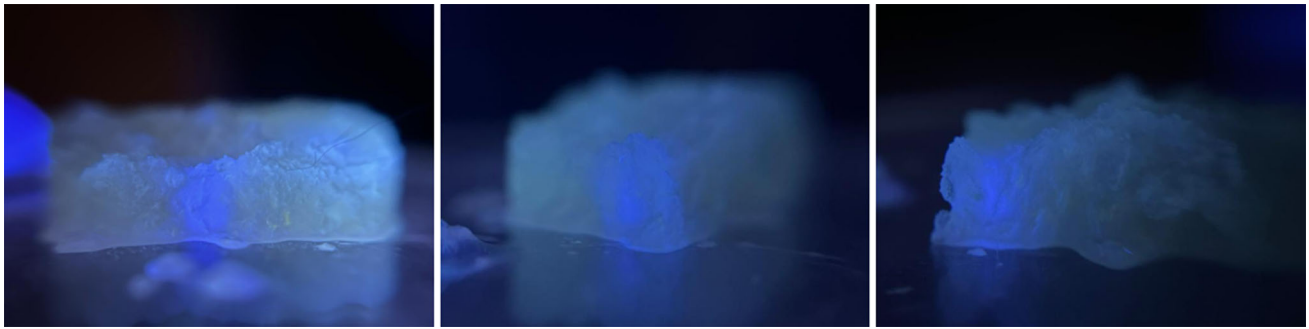


**Fig. 3** Photos of the hydrogel after taken after the fluorescent marker's (a bright blue spot) spread: its cross sections by planes through the centre of injection demonstrate that the vertical distribution is homogeneous, and one can analyse the radial spread only

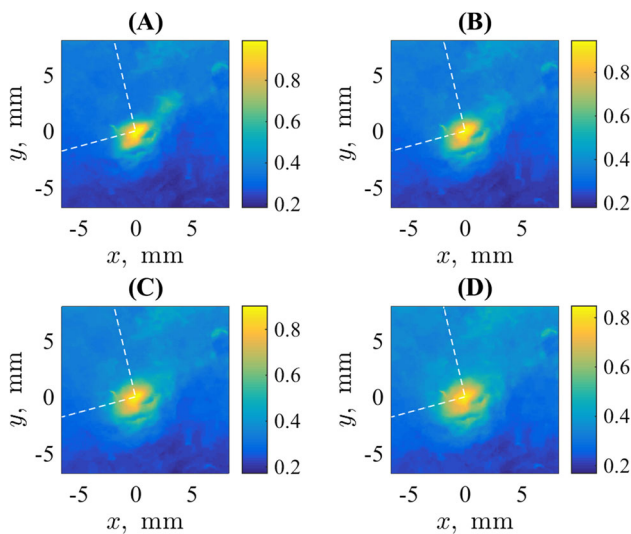


**Fig. 4** Scaled fluorescence intensity of marker's spread record for the time moments 1 min (A), 6 min (B), 11 min (C), and 16 min (D) after the beginning of video recording. The dashed lines bound to the angular region with the relatively rotational uniform part of the distribution analysed especially

spot of dispersed marker concentration but also separately the part, which is relatively angle-invariant. Its boundaries are denoted by the dashed lines in Fig. 4. The computational procedure was organised as follows. The  $400 \times 400$  matrix (with the scale  $0.037 \text{ mm/px}$ ) of recorded intensities was re-plotted from Cartesian to polar coordinates with the centre aligned with the location, where the marker was initially introduced. The images were re-scaled into a rectangular matrix, from which the part  $125 \times 530$  pixels respectively to the pair of radial and angular coordinates was considered; here the scale factor for the radial coordinates is equal to  $0.013 \text{ mm/px}$ , and the angular range covers the full circle  $[0, 2\pi)$ .

The radial dependencies of the fluorescence intensity, which mimics the concentration distribution, were found via the angle averaging for two cases: (a) inside of the angle denoted in Fig. 4 by the white dashed line

and for the full angle. The corresponding dependencies normed to unity in the point of maximum are shown in Fig. 5A and B, respectively.

Note that that the normal diffusion from a point source in a uniform medium with the effective diffusion coefficient  $D$  satisfies in the Gaussian distribution for the concentration

$$P(r, t) \propto e^{-\frac{r^2}{4Dt}}. \quad (1)$$

When the distribution is normalised to the unity at the maximum, which is in the point  $r = 0$ , the logarithm of Eq. (1) is a linear function respectively to the radial distance squared. Figure 5A demonstrates namely such a behaviour, which is especially seen at short time moments. After a while, the central part (small  $r$ ) weakly changed its slope since it is saturated with the fluorescent marker but the tails of distribution are also linear. This indicates normal (Brownian (Fickian)) character of diffusion within angle region, where the recorded distribution does not have visual peculiarities, see Fig. 4.

On the contrary, the black line in Fig. 5B is linear not as a function of  $r^2$  but as a function of  $r$  within a significant interval of radial coordinate (see the grey straight line providing visual guidance). This dependence implies the Laplace distribution

$$P(r, t) \propto e^{-\frac{r}{4\langle D \rangle t^{1/2}}}, \quad (2)$$

where  $\langle D \rangle$  is an effective diffusivity of the so-called Brownian-yet-not-Gaussian (BnG) diffusion model.

However, the tail of the experimental distribution looks parabolic. Moreover, the beginning of such curve shifts closer to the origin of coordinates with time that indicates asymptotic development of the standard diffusive spread. Note that such a behaviour is typical for the BnG diffusion. The essence of this process consists of an absence of a unique diffusion coefficient but rather a distribution  $p(D)$  for mixture of different local diffusivities within the concept of superstatistics pioneered by Beck and Cohen [30], see also the review [31]. The resulting registered concentration distribution is a result of

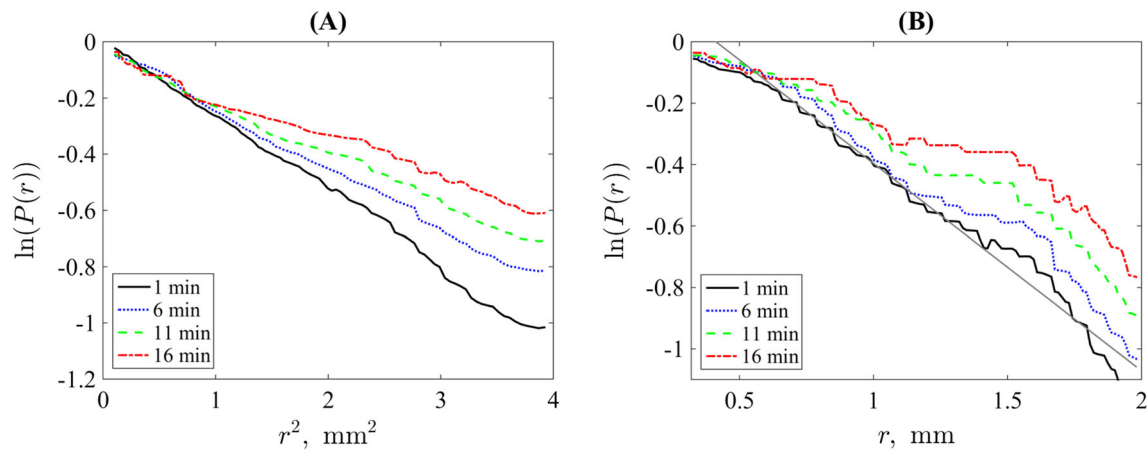


**Fig. 5** The logarithms of the average radial distributions of the fluorescence intensity normalized to unity at the maximum for sequential time moments: **A** as a function of the radial distance squared within the angular interval highlighted in Fig. 4 and **B** as a radial distance after averaging over the full angles; here the grey straight line is added to visual guidance

averaging

$$P(r, t) = \int_0^{\infty} p(D) \frac{e^{-\frac{r^2}{4Dt}}}{(4\pi Dt)^{N/2}} dD, \quad (3)$$

where  $N$  is the dimension of space; in the case of uniformity of the instant vertical spread as visible in Fig. 3; our situation is effectively two-dimensional,  $N = 2$ .

Since curves in Fig. 5B are obtained after averaging over the full range  $[0, 2\pi)$ , where one can clearly see in Fig. 4 different degree of the marker's percolation, i.e. the applied averaging already averages over the regions with different transport properties.

Respectively, the transition between the effective Laplacian distribution, Eq. (2), to the effective Gaussian distribution, Eq. (2), may originate either from relaxation of the local diffusivities with time (the “diffusing diffusivity” model proposed by Chubynsky and Slater [32] and substantiated from the superstatistical point of view in the work [33]) or from homogenization of a static irregular structure when the marker spreads over an area with radius much more exceeding correlation lengths of local inhomogeneities (the “quenching disorder model” explored in the work [34]).

Note finally that such non-conventional picture of diffusion is similar to the cases registered in some studies of transport processes in the brain's extracellular space via the Magnetic Resonance Imaging [4, 29], where experimental distributions in the brain's tissue clearly deviate from the Gaussian distribution. In particular, Fig. 6 gives examples of the distributions of the MRI contrast agents in living rodent brain. One can see not only visual similarity of the diffusive spot in the inset of Fig. 6 and, say, Fig. 4B but also the evidence of a functional form of the Laplace distribution (2) when the data obtained in the work [4] are re-plotted in semi-logarithmic scale. Thus, the proposed hydrogel medium already mimics the realistic brain's parenchyma.

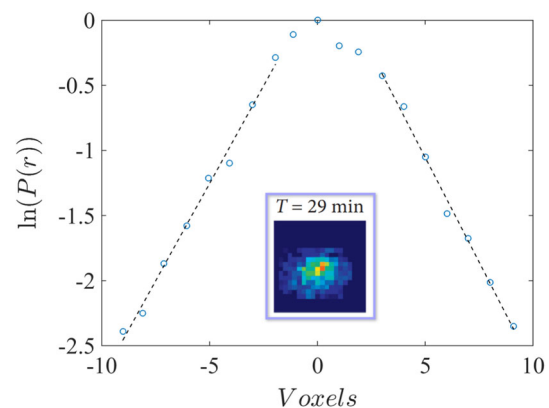


**Fig. 6** An example of the distribution of Gadovist (also known under its chemical name gadobutrol) in rat's brain plotted basing on the digitised data from [4] (The referenced work was published under the Creative Commons Attribution License); the dashed lines are shown for the visual guidance highlighting linearity in semi-logarithmic co-ordinates. The inset shows the MultiHance contrast agent spatial distribution under the same conditions and the time moment

## 5 Conclusion

In our work, we presented an experimental model of the brain parenchyma in which we investigated particle transport in an initial approximation. By syntheses of the “experimental parenchyma,” we took into account the gel-like porous consistency as well as the presence of properties for binding sufficient amounts of water. Considering the marker spread allowed us not only estimate the effective diffusion coefficient of the synthesised substance but also analyse possible peculiarities of the transport process similar to those, which are detected in the real brain tissue. In particular, we argued that the complex structure of hydrogel can lead to the emergence of the “Brownian-yet-not-Gaussian”

**Table 1** Summary of similarity of the developed hydrogel phantom to the biological brain tissue

Brain	Hydrogel
The brain's extracellular matrix: glycosaminoglycans (e.g. hyaluronan), proteoglycans (e.g. neurocan, brevican, versican and aggrecan), glycoproteins (e.g. tenascin-R), and low levels of fibrous proteins (e.g. collagens I, III, IV, V, VI, fibronectin, and vitronectin) [35]	The basic components: collagens I, III, hyaluronic acid (nonsulfated glycosaminoglycan) with small amount of phospholipids (lecitin) and short proteins
Water content: 80 – 85% [36]	Water content: up to 91%
ECM consists of 10–20% of the total volume [37]	Collagen network (wet) consists of about 10–15 % of the total volume
Gadobutrol's apparent diffusion coefficient ranging as $D \approx (150 - 170) (\text{m}^2/\text{s})$ in the human brain's grey matter [38]	The diffusivity of acridon-2-sulfonsaure is determined as about $D = 127 \mu(\text{m})^2/\text{s}$ [39]

diffusion, which is of recent interest in the biophysical problems.

Based on our study, we summarised the properties of the brain parenchyma and the material imitating it (see Table 1). It should be noted that in terms of water composition, the experimental model is very close to the characteristics of the brain. The same conclusion can be made in relation to diffusion estimation and to the collagen network, which imitates the extracellular matrix of the brain parenchyma. There are significant differences in the composition comparison, especially since the bio-organic composition of the brain parenchyma is organised into a layered hierarchical network [11], but modification of our experimental model may be a good prospect for new studies.

**Acknowledgements** This work was supported by Grant of Russian Science Foundation, project #22-15-00143.

**Data availability statement** The original video recordings can be provided from the corresponding author on reasonable request.

**Declarations**

**Conflict of interest** The authors declare that they have no conflict of interest.

## References

1. C. Nicholson, S. Hrabětová, Brain extracellular space: the final frontier of neuroscience. *Biophys. J.* **113**, 2133–2142 (2017). <https://doi.org/10.1016/j.bpj.2017.06.052>
2. C. Nicholson, The secret world in the gaps between brain cells. *Phys. Today* **75**, 26–32 (2022). <https://doi.org/10.1063/PT.3.4999>
3. J.J. Iliff, M. Wang, Y. Liao, B.A. Plogg, W. Peng, G.A. Gundersen, H. Benveniste, G.E. Vates, R. Deane, S.A. Goldman, E.A. Nagelhusand, M. Nedergeerd, A paravascular pathway facilitates CSF flow through

- the brain parenchyma and the clearance of interstitial solutes, including amyloid  $\beta$ . *Sci. Transl. Med.* **4**, 111–147 (2012). <https://doi.org/10.1126/scitranslmed.3003748>
4. A. Conti, R. Magnin, M. Gerstenmayer, N. Tsapis, E. Dumont, O. Tillement, F. Lux, D. Le Bihan, S. Mériaux, S. Della Penna, B. Larrat, Empirical and theoretical characterization of the diffusion process of different gadolinium-based nanoparticles within the brain tissue after ultrasound-induced permeabilization of the blood-brain barrier. *Contrast Media Mol. Imaging* **2019**, 6341545 (2019). <https://doi.org/10.1155/2019/6341545>
5. E.B. Postnikov, A.I. Lavrova, D.E. Postnov, Transport in the brain extracellular space: diffusion, but which kind? *Int. J. Mol. Sci.* **23**(20), 12401 (2022). <https://doi.org/10.3390/ijms232012401>
6. K.E. Holter, B. Kehlet, A. Devor, T.J. Sejnowski, A.M. Dale, S.W. Omholt, O.P. Ottersen, E.A. Nagelhus, K.-A. Mardal, K.H. Pettersen, Interstitial solute transport in 3D reconstructed neuropil occurs by diffusion rather than bulk flow. *Proc. Natl. Acad. Sci. USA* **114**, 9894–9899 (2017). <https://doi.org/10.1073/pnas.1706942114>
7. L.A. Ray, J.J. Heys, Fluid flow and mass transport in brain tissue. *Fluids* **4**, 196 (2019). <https://doi.org/10.3390/fluids4040196>
8. M.K. Rasmussen, H. Mestre, M. Nedergaard, Fluid transport in the brain. *Physiol. Rev.* **102**, 1025–1151 (2022). <https://doi.org/10.1152/physrev.00031.2020>
9. S.B. Hladky, M.A. Barrand, The glymphatic hypothesis: the theory and the evidence. *Fluids Barriers CNS* **19**, 9 (2022). <https://doi.org/10.1186/s12987-021-00282-z>
10. F.N. Soria, C. Miguelez, O. Peñagarikano, J. Tønnesen, Current techniques for investigating the brain extracellular space. *Front. Neurosci.* **14**, 570750 (2020). <https://doi.org/10.3389/fnins.2020.570750>
11. O. Chaudhuri, J. Cooper-White, P.A. Janmey, D.J. Mooney, V.B. Shenoy, Effects of extracellular matrix viscoelasticity on cellular behaviour. *Nature* **584**(7822), 535–546 (2020). <https://doi.org/10.1038/s41586-020-2612-2>
12. S. Hrabětova, Brain extracellular space changes dynamically during physiological and pathological neuronal activity. *Biophys. J.* **121**, 28 (2022). <https://doi.org/10.1016/j.bpj.2021.11.2572>

13. R. Rauti, N. Renous, B.M. Maoz, Mimicking the brain extracellular matrix in vitro: a review of current methodologies and challenges. *Isr. J. Chem.* **60**, 1141–1151 (2020). <https://doi.org/10.1002/ijch.201900052>
14. Z.-J. Chen, G.T. Gillies, W.C. Broaddus, S.S. Prabhu, H. Fillmore, R.M. Mitchell, F.D. Corwin, P.P. Fatouros, A realistic brain tissue phantom for intraparenchymal infusion studies. *J. Neurosurg.* **101**, 314–322 (2004). <https://doi.org/10.3171/jns.2004.101.2.0314>
15. E. Syková, C. Nicholson, Diffusion in brain extracellular space. *Physiol. Rev.* **88**, 1277–1340 (2008). <https://doi.org/10.1152/physrev.00027.2007>
16. R. Pomfret, G. Miranpuri, K. Sillay, The substitute brain and the potential of the gel model. *Ann. Neurosci.* **20**, 118–122 (2013). <https://doi.org/10.5214/ans.0972.7531.200309>
17. E. Axpe, G. Orive, K. Franze, E.A. Appel, Towards brain-tissue-like biomaterials. *Nat. Commun.* **11**, 3423 (2020). <https://doi.org/10.1038/s41467-020-17245-x>
18. Z. Tan, J.P. Ewen, A.E. Forte, S. Galvan, E. De Momi, F. Rodriguez y Baena, D. Dini, What does a brain feel like? *J. Chem. Educ.* **97**, 4078–4083 (2020). <https://doi.org/10.1021/acs.jchemed.0c00957>
19. A. Tejo-Otero, F. Fenollosa-Artés, I. Achaerandio, S. Rey-Vinolas, I. Buj-Corral, M.Á. Mateos-Timoneda, E. Engel, Soft-tissue-mimicking using hydrogels for the development of phantoms. *Gels* **8**, 40 (2022). <https://doi.org/10.3390/gels8010040>
20. Y. Bouattour, V. Sautou, R. Hmede, Y. El Ouadhi, D. Gouot, P. Chennell, Y. Lapusta, F. Chapelle, J.-J. Lemaire, A minireview on brain models simulating geometrical, physical, and biochemical properties of the human brain. *Front. Bioeng. Biotechnol.* **10**, 818201 (2022). <https://doi.org/10.3389/fbioe.2022.81820>
21. F. Hucho, *Neurochemistry* (Fundamentals and Concepts. VCH, Weinheim, 1986)
22. C. Nicholson, P. Kamali-Zare, L. Tao, Brain extracellular space as a diffusion barrier. *Comput. Vis. Sci.* **14**, 309–325 (2011). <https://doi.org/10.1007/s00791-012-0185-9>
23. J.A. DeQuach, S.H. Yuan, L.S.B. Goldstein, K.L. Christman, Decellularized porcine brain matrix for cell culture and tissue engineering scaffolds. *Tissue Eng. Part A* **17**, 2583–2592 (2011). <https://doi.org/10.1089/ten.tea.2010.0724>
24. V.M. Runge, S. Aoki, W.G. Bradley Jr., K.-H. Chang, M. Essig, L. Ma, J.S. Ross, A. Valavanis, Magnetic resonance imaging and computed tomography of the brain—50 years of innovation, with a focus on the future. *Invest. Radiol.* **50**, 551–556 (2015). <https://doi.org/10.1097/RLI.0000000000000170>
25. G. Boulouis, A. Morotti, A. Charidimou, D. Dowlatshahi, J.N. Goldstein, Noncontrast computed tomography markers of intracerebral hemorrhage expansion. *Stroke* **48**, 1120–1125 (2017). <https://doi.org/10.1161/STROKEAHA.116.015062>
26. J. Ślęzak, S. Burov, From diffusion in compartmentalized media to non-Gaussian random walks. *Sci. Rep.* **11**, 5101 (2021). <https://doi.org/10.1038/s41598-021-83364-0>
27. M.C. Papadopoulos, J.K. Kim, A.S. Verkman, Extracellular space diffusion in central nervous system: anisotropic diffusion measured by elliptical surface photobleaching. *Biophys. J.* **89**, 3660–3668 (2005). <https://doi.org/10.1529/biophysj.105.068114>
28. F. Xiao, C. Nicholson, J. Hrabe, S. Hrabětová, Diffusion of flexible random-coil dextran polymers measured in anisotropic brain extracellular space by integrative optical imaging. *Biophys. J.* **95**, 1382–1392 (2008). <https://doi.org/10.1529/biophysj.107.124743>
29. S. Mériaux, A. Conti, B. Larrat, Assessing diffusion in the extra-cellular space of brain tissue by dynamic MRI mapping of contrast agent concentrations. *Front. Phys.* **6**, 38 (2018). <https://doi.org/10.3389/fphy.2018.00038>
30. C. Beck, E.G.D. Cohen, Superstatistics. *Phys. A* **322**, 267–275 (2003). [https://doi.org/10.1016/S0378-4371\(03\)00019-0](https://doi.org/10.1016/S0378-4371(03)00019-0)
31. R. Metzler, Superstatistics and non-Gaussian diffusion. *Eur. Phys. J. Special Topics* **229**, 711–728 (2020). <https://doi.org/10.1140/epjst/e2020-900210-x>
32. M.V. Chubynsky, G.W. Slater, Diffusing diffusivity: a model for anomalous, yet Brownian, diffusion. *Phys. Rev. Lett.* **113**, 098302 (2014). <https://doi.org/10.1103/PhysRevLett.113.098302>
33. A.V. Chechkin, F. Seno, R. Metzler, I.M. Sokolov, Brownian yet non-Gaussian diffusion: from superstatistics to subordination of diffusing diffusivities. *Phys. Rev. X* **7**, 021002 (2017). <https://doi.org/10.1103/PhysRevX.7.021002>
34. E.B. Postnikov, A. Chechkin, I.M. Sokolov, Brownian yet non-Gaussian diffusion in heterogeneous media: from superstatistics to homogenization. *New J. Phys.* **22**, 063046 (2020). <https://doi.org/10.1088/1367-2630/ab90da>
35. D. Lam, H.A. Enright, J. Cadena, S.K.G. Peters, A.P. Sales, J.J. Osburn, D.A. Soscia, K.S. Kulp, E.K. Wheeler, N.O. Fischer, Tissue-specific extracellular matrix accelerates the formation of neural networks and communities in a neuron-glia co-culture on a multi-electrode array. *Sci. Rep.* **9**, 4159 (2019). <https://doi.org/10.1038/s41598-019-40128-1>



36. A.-M. Oros-Peusquens, R. Loução, Z. Abbas, V. Gras, M. Zimmermann, N.J. Shah, A single-scan, rapid whole-brain protocol for quantitative water content mapping with neurobiological implications. *Front. Neurol.* **10**, 1333 (2019). <https://doi.org/10.3389/fneur.2019.01333>
37. E.E. Benarroch, Extracellular matrix in the CNS: dynamic structure and clinical correlations. *Neurology* **85**, 1417–1427 (2015). <https://doi.org/10.1212/WNL.0000000000002044>
38. L.M. Valnes, S.K. Mitusch, G. Ringstad, P.K. Eide, S.W. Funke, K.-A. Mardal, Apparent diffusion coefficient estimates based on 24 hours tracer movement support glymphatic transport in human cerebral cortex. *Sci. Rep.* **10**, 9176 (2020). <https://doi.org/10.1038/s41598-020-66042-5>
39. A.S. Vanina, A.V. Sychev, E.V. Grekhnyova, E.B. Postnikov, A collagen network-based hydrogel phantom for testing models of the metabolite transport in the brain parenchyma. In: 2022 Fourth International Conference Neurotechnologies and Neurointerfaces (CNN), pp. 212–214 (2022). <https://doi.org/10.1109/CNN56452.2022.9912549>

Springer Nature or its licensor (e.g. a society or other partner) holds exclusive rights to this article under a publishing agreement with the author(s) or other rightsholder(s); author self-archiving of the accepted manuscript version of this article is solely governed by the terms of such publishing agreement and applicable law.